URSI - RCRS 2022, IIT (Indore), India, 1 - 4 December, 2022

Single-pulse and average emission characteristics of PSR J1820-0427

Parul Janagal*(1), Manoneeta Chakraborty(1), N. D. Ramesh Bhat(2), S. J. McSweeney(2)
(1) Department of Astronomy, Astrophysics, and Space Engineering, Indian Institute of Technology Indore, Indore 453552, India
(2) International Centre for Radio Astronomy Research, Curtin University, Bentley, WA 6102, Australia

Abstract

We have conducted a detailed study of pulse-to-pulse variation in the bright long-period pulsar PSR J1820-0427, using high-quality data from the upgraded Giant Metrewave Radio Telescope (uGMRT) and the Murchison Widefield Array (MWA). We have investigated several aspects of the pulsar emission, including the pulse energy distribution and its relation to the Stochastic Growth Theory (SGT), the spectral index and its pulse-to-pulse variability, and the profile evolution across the ~170 MHz to 750 MHz range, including the effects of temporal broadening arising from multi-path scattering due to the ISM. We have also studied the global spectral behaviour of the pulsar, suggesting a low-frequency turnover at frequencies below 300 MHz. Furthermore, we demonstrate a new approach for calibrating beamformed data from the uGMRT and utilise these calibrated flux densities for exploring the pulse-to-pulse spectral index variability.

1. Introduction

The discovery of pulsars is considered to be one of the significant findings in astronomy in the last century. Pulsars are rotating neutron stars which are sites of highly energetic physical processes, owing to the extremely high densities, strong gravity and magnetic fields, along with a high rotation period. The emission process behind these periodic pulses has remained an open question and is widely studied. Radio pulsars are known to exhibit a variety of effects related to amplitude modulation in single pulses. Despite the variation in shape and intensity of single pulses, the average pulsar profile stays stable over the long term. In contrast to the averaged profile, single pulses can help study the plasma variability arising from the turbulent and dynamic nature of the plasma. Detailed study of these individual pulses can help put constraints on the theoretical models of emission and the distribution of emitting particles, bringing additional insight into the pulsar emission physics. The single pulse study of pulsars necessitates exceptionally high-quality data, such that every single pulse is significantly detectable. J1820-0427 is a bright "normal" pulsar with a period of 0.598 seconds and a dispersion measure (DM) of 84.435 pc cm^{-3}. The pulsar exhibits unorganised amplitude modulation. The brightness and the variable single pulse characteristics of the source make it an interesting candidate for studying the emission and basic properties of pulsars. Using the high-quality wideband multi-frequency observations from MWA and uGMRT, we have studied the complex frequency dependence of single pulses in detail.

2. Observation and Calibration

In this work, we have covered an almost contiguous wide-frequency range of 170 - 750 MHz using MWA and uGMRT.

2.1 MWA

At the time of our observations, MWA operated in the extended array configuration, comprising 128 4x4 tiles, with a contiguous bandwidth of 30.72 MHz, spread over 24 available individual coarse channels across the centre frequency of 185 MHz. The data were recorded using the Voltage Capture System (VCS) [1]. In this mode, the channelised voltages are recorded from each tile, which are summed coherently after calibration. The pulsar was observed for 45 minutes, giving close to 4500 pulses.

The raw voltages recorded by the MWA can be used to create visibilities further to obtain the images and source flux at the observed frequency. The xGPU software correlators were used to create "visibilities" at 1s time resolution from the raw voltages recorded from the MWA tiles. These visibilities are converted into CASA (Common Astronomy Software Applications) measurement set [2] using the COTTER software [3] and were further RFI (Radio Frequency Interference) excised. The calibration solutions were obtained from the Murchison Widefield Array All-Sky Virtual Observatory (MWA-ASVO) [4]. WSCLEAN was used to form images. The final image generated was 8192 by 8192 pixels, with a pixel size of 0.049 degrees/pixel, producing 40^o x 40^o images. The mean standard deviation of the Stokes I image used for processing is ~5 mJy/beam around the centre of the image. For PSR J1820-0427, the flux density at 185 MHz was 790 +/- 63 mJy.

2.2 uGMRT

We used the uGMRT to observe the pulsar simultaneously at Band 3 (300-500 MHz) and Band 4 (550-750 MHz) of the uGMRT in the phased array mode. The data were recorded with a time resolution of 327.68 μs, and a bandwidth of 200 MHz spread over 4096 frequency channels with a resolution of 48 kHz. The observations were made at two epochs, ~10 days apart, at both frequency bands. The pulsar was observed for roughly one hour in each epoch, giving close to 6000 pulses per epoch. The first level processing was done using DSPSR. Single pulse frequency scrunched archives were made using routines from PSRCHIVE. The stray RFI occurrences were excised using the 'pazi' subroutine of PSRCHIVE.

The uGMRT also simultaneously recorded the cross-correlated visibilities of the pulsar field. The data were stored in the .lta (Long Term Accumulation) format. The visibility data were reduced using the SPAM (Source Peeling and Atmospheric Modeling) [5] pipeline and CASA. We first used the SPAM pipeline to obtain the stokes I continuum image. After converting the files in the .UVFITS format, SPAM derives the calibration and flagging information from the primary calibrators. These solutions are then applied to the target. SPAM automatically split the data into smaller subbands, and each subband was processed independently. Band 3 observations were automatically divided into six subbands and Band 4 observations in four subbands. Each SPAM pipeline run on a sub-band yielded a final image and a calibrated visibility data set (.SP2B.CAL.RR.UVFITS). Imaging was performed on the final calibrated data using the CASA task 'tclean' to obtain the source flux density.

We further used the simultaneously recorded cross-correlated visibilities to calibrate the beamformed (phased array) uGMRT data of the pulsar. This allows us to study the spectral behaviour of every single pulse from the pulsar and understand the short-scale physical processes. The flux calibration of beamformed data of pulsars can be challenging using telescope arrays. In general, such flux calibrations are performed using noise diodes, commonly found in single-dish telescopes, but are uncommon in arrays. In this work, we have employed a novel approach to use the cross-correlated visibilities to calibrate the single pulses from the beamformed data. This exercise of calibrating the single pulses using imaging flux was only carried out for the uGMRT data, owing to a single pulse S/N of ~100.

For performing the calibration of single pulse data using the simultaneous imaging data, the underlying assumption is that the sensitivity of the telescope is the same in both modes of operation: phased array and interferometer. This implies that the RMS noise of the receiver is identical to the phased array beam and the cross-correlated visibilities. Therefore, using the RMS from the image and applying a boosting factor, we calculated the equivalent RMS of the off-pulse region of the average pulsar profile as -

$$RMS_{PA}(mJy) = \sqrt{\frac{P - t_{samp}}{t_{samp}}}\, RMS_{Img}\,(mJy)$$

where P is the pulsar period, and t_{samp} is the pulsar sampling time, which is equivalent to the width of a phase bin. This boosting factor accounts for the fraction of the pulsar period during which no emission was seen from the pulsar, i.e., when the pulsar was "off" in its duty cycle. Further, according to our assumptions, this RMS_{PA} should be the same as the RMS noise of the off pulse region in the averaged profile (arbitrary units). Using the average profile, we defined the off-pulse region and calculated the area under the curve $RMS_{offpulse}$ in arbitrary units. We then scaled all the data points in the whole time series by $\frac{RMS_{PA}}{RMS_{offpulse}}$ to bring each value to physical units (mJy). The calibrated time series was then used to perform all the analyses henceforth.

3. Analysis and Results

3.1 Pulsar Profile

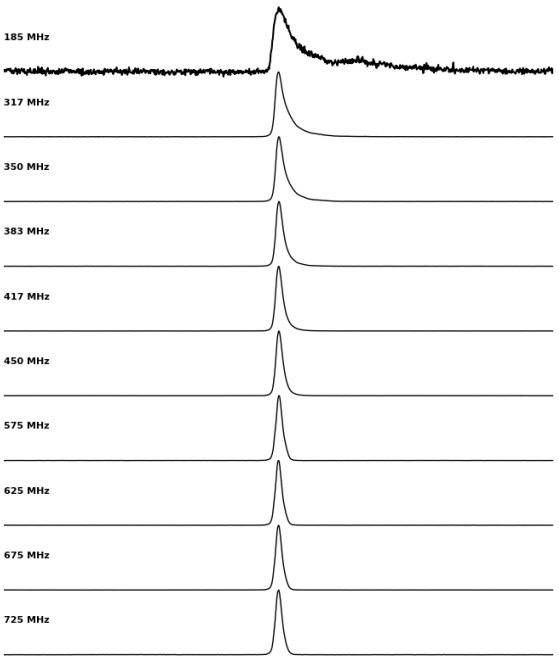

Figure 1. Profile evolution of PSR J1820-0427 from 185 MHz to 725 MHz, from observations made with the MWA and the uGMRT. uGMRT data were sub-divided into multiple sub-bands. The unprecedentedly high-quality of uGMRT data has enabled a detailed exploration of pulse-to-pulse variability in the emission properties of the pulsar. The profile at the MWA

frequency band (170-200 MHz) shows a secondary feature near the trailing side, for which no counterparts are seen in uGMRT bands.

Average profiles of PSR J1820-0427 at multiple observing frequencies are shown in figure 1, with frequency increasing from top to bottom. The x-axis shows the pulsar phase, where the peak of every average profile is centred on 0.5. The uGMRT data, originally taken with 200 MHz bandwidth, was divided into multiple subbands to study the frequency evolution of the pulsar. The excellent quality of the uGMRT data can also be seen clearly in each of the averaged profiles at frequencies from 317 to 725 MHz, where the off-pulse noise is very close to zero. The pulsar profile at the MWA frequency band (170-200 MHz) shows a secondary feature near the trailing end of the profile, close to phase ~0.62, for which no counterparts are seen in the GMRT bands.

3.2 Global Spectral Evolution

Using the large bandwidth of our data, we studied the simultaneous frequency evolution of pulsar properties in great detail. Using SPAM and CASA, we obtained the flux density values of J1820-0427 at multiple frequency subbands. We collated all the flux density measurements from this work and the existing literature and fit the resultant spectrum as shown in figure 2. The spectral fitting procedure is performed using PULSAR SPECTRA (Swainston et al., *submitted*), an open-source database of published spectral data. Contrary to the published literature [6], we have found that a low-frequency turn-over power-law function best fits the pulsar's spectral behaviour.

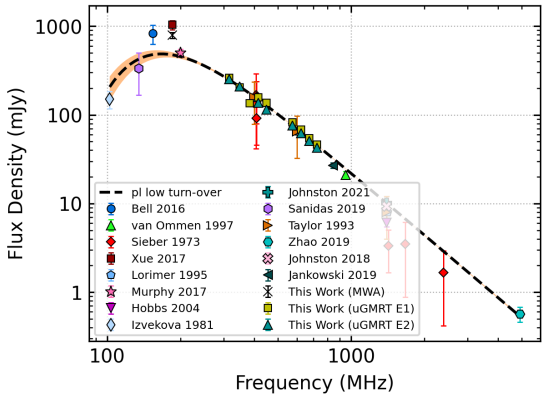

Figure 2. Spectrum of PSR J1820-0427, obtained from measurements made with the MWA (185 MHz) and the uGMRT (300-750 MHz), along with several others from the published literature. The Black dashed line is the best-fitting model to the data, and the orange shaded envelope is the 1σ uncertainty of the best-fitting model.

3.3 Pulse Energy Distribution

The investigation of pulse energy distribution provides insights into the dynamic radio pulsar emission mechanism and the physical state of the pulsar magnetosphere. The distribution of single pulse energies can provide a window to the instantaneous state of pulsar plasma and the kind of emission mechanisms.

We determined the on-pulse region in each observation visually using the average profile. The pulse energy was then calculated for every single pulse by integrating the calibrated flux in the on-pulse region. Since the flux density is calibrated for every single pulse, the pulse energy will have units of mJy ms. A histogram of pulse energies was then constructed to study the distribution. We found that a log-normal distribution best describes the pulse energy distribution at all the observed frequencies. We fitted a log-normal model to the observational data using a least-squares fitting method, defined using the parameters μ and σ:

$$N(E) = \frac{A}{E} e^{\frac{-(\ln E - \mu)^2}{2\sigma^2}}$$

where E is the pulse energy and A is the scaling factor. μ and σ are the mean and standard deviation of the natural logarithm of the energy distribution, N(E).

The Stochastic Growth Theory (SGT) predicts a log-normal distribution of the observed single pulse energies. It describes self-consistently interacting systems where the interactions occur in an independent homogeneous medium and introduce distance and time scales. Our work, for the first time, studies such an evolution of pulse energies over a large frequency range (300-750 MHz). We have found that the pulse energy distribution is unchanged at large radio frequency ranges, though there is certain evolution of the intrinsic parameters. From our single pulse analysis of J1820-0427, the pulse energy distribution indicates a small number of strong energy pulses, albeit not giant pulses.

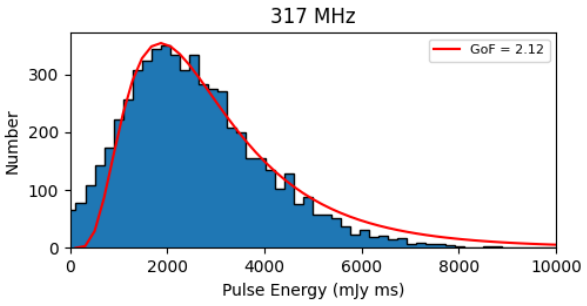

Figure 3. Pulse energy histogram of PSR J1820-0427 at 317 MHz from Epoch 1 observations of uGMRT. In support of theories like SGT, we found a log-normal distribution of pulse energies, consistent at all frequencies (not shown here). The histogram is fitted with a log-normal distribution shown as the red curve. Histograms at all the observed frequencies show similar log-normal behaviour with different parameters.

3.4 Pulse-to-pulse Variability

Using the calibrated single pulse data, we studied the spectral behaviour of every single pulse over the extensive frequency range. We calculated the pulse-to-pulse spectral index (SI) to examine the single pulse variability. The wide variation in single pulse spectral index, with no correlation with the following pulse, indicated a physical process disorganised at short time scales, as claimed by the SGT, despite a global trend at large averaged time scales.

The single pulse variability was further confirmed by calculating the modulation index, a number used to quantify the pulse to pulse intensity modulation, for all data at all the observed frequencies. We found that the modulation index is close to 0.5, with variations along the pulse phase.

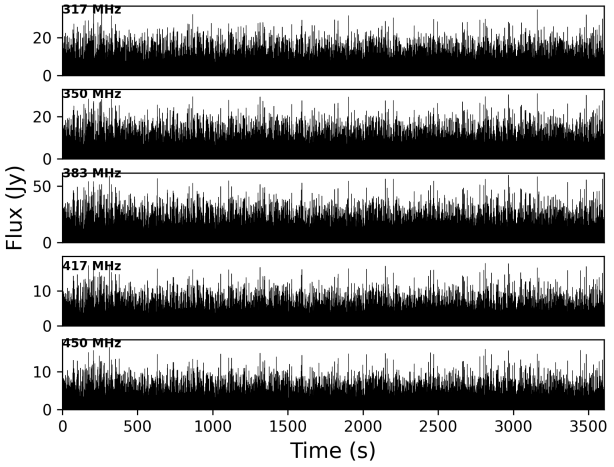

Figure 4. Calibrated single-pulse train for PSR J1820-0427 at multiple observation frequencies for uGMRT Epoch 1. The high variability of single pulses can be seen, which decreases with higher frequency. A single high amplitude pulse also emerges at higher frequencies, showing a peculiar spectral index.

Owing to the wide observing bandwidth, we also inspected the correlation between the intensities at consecutive frequencies using the calibrated single pulse flux densities. We found that the correlation between closer frequency pairs is tighter. In addition, there appears to be a general tendency for brighter pulses to show a steepening of the spectral index. This could indicate more coherence in the emission process for bright pulses. An intermediate category of pulses, between normal and giant pulses, also conforms with the claim of strong single pulses of PSR J1820-0427 from the pulse energy histogram.

4. Conclusion

We have performed the first simultaneous multi-frequency single-pulse analysis of a slow pulsar PSR J1820-0427. We have used data from MWA at 185 MHz, which is a precursor for Square Kilometer Array (SKA), and from uGMRT at Band-3 (300-500 MHz) and Band-4 (550-750 MHz), a SKA pathfinder. Such low-frequency studies are crucial for constraining the spectral characteristics of pulsar emission at frequencies below 300 MHz, where SKA-Low will operate. In our study, we have devised a novel method to calibrate single pulse data using the simultaneously recorded visibility data and applied it to the high-quality uGMRT data. We have found that the single pulse energies are best described using a log-normal distribution at a wide range of observed frequencies from 300 to 750 MHz. We studied the pulse-to-pulse variability shown by the pulsar, which indicated an emission process unorganised at time scales shorter than the pulsar period. A few occurrences of very bright pulses were noted, which were found not to be giant pulses upon further analysis. The steep spectrum of high-intensity pulses indicates increased coherence in the emission.

5. Acknowledgements

PJ acknowledges the Senior Research Fellowship awarded by the Council of Scientific & Industrial Research, India. We thank the staff of the GMRT and MWA who have made these observations possible. The GMRT is run by the National Centre for Radio Astrophysics of the Tata Institute of Fundamental Research.

6. References

1. Tremblay, S. E., “The High Time and Frequency Resolution Capabilities of the Murchison Widefield Array”, *Publications of the Astronomical Society of Australia*, vol. 32, 2015. doi:10.1017/pasa.2015.6.
2. McMullin, J. P., Waters, B., Schiebel, D., Young, W., and Golap, K., “CASA Architecture and Applications”, in *Astronomical Data Analysis Software and Systems XVI*, 2007, vol. 376, p. 127.
3. A. R. Offringa et. al., “The Low-Frequency Environment of the Murchison Widefield Array: Radio-Frequency Interference Analysis and Mitigation,” *Publications of the Astronomical Society of Australia*, vol. 32, p. e008, 2015.
4. M. Sokolowski et al., “Calibration and Stokes Imaging with Full Embedded Element Primary Beam Model for the Murchison Widefield Array,” *Publications of the Astronomical Society of Australia*, vol. 34, p. e062, 2017.
5. Intema, H. T., “SPAM: A data reduction recipe for high-resolution,low-frequency radio-interferometric observations”, in *Astronomical Society of India Conference Series*, 2014, vol. 13, p. 469.
6. S. Burke-Spolaor et al., The High Time Resolution Universe Pulsar Survey – V. Single-pulse energetics and modulation properties of 315 pulsars, *Monthly Notices of the Royal Astronomical Society*, Volume 423, Issue 2, June 2012, Pages 1351–1367, https://doi.org/10.1111/j.1365-2966.2012.20998.x